Axial Flux Permanent Magnet Brushless Machines

Axial Flux Permanent Magnet Brushless Machines

by

JACEK F. GIERAS
United Technologies Research Center,
East Hartford, Connecticut, U.S.A.

RONG-JIE WANG
University of Stellenbosch,
Stellenbosch, Western Cape, South Africa

and

MAARTEN J. KAMPER
University of Stellenbosch,
Stellenbosch, Western Cape, South Africa

KLUWER ACADEMIC PUBLISHERS
NEW YORK, BOSTON, DORDRECHT, LONDON, MOSCOW

eBook ISBN: 1-4020-2720-6
Print ISBN: 1-4020-2661-7

Created in the United States of America

Visit Springer's eBookstore at: http://ebooks.springerlink.com
and the Springer Global Website Online at: http://www.springeronline.com

Contents

Preface

The drop in prices of rare-earth permanent magnet (PM) materials and progress in power electronics have played an important role in the development of PM brushless machines in the last three decades. These machines have recently become mature and their high efficiency, power density and reliability has led to PM brushless machines successfully replacing d.c. commutator machines and cage induction machines in many areas.

The axial flux PM (AFPM) brushless machine, also called the disc-type machine, is an attractive alternative to its cylindrical radial flux counterpart due to the pancake shape, compact construction and high torque density. AFPM motors are particularly suitable for electrical vehicles, pumps, valve control, centrifuges, fans, machine tools, hoists, robots and manufacturing. They have become widely used for low-torque servo and speed control systems. The application of AFPM machines as generators is justified in wind turbines, portable generator sets and road vehicles. The power range of AFPM brushless machines is now from a fraction of a watt to sub-MW.

Disc-type rotors can be embedded in power-transmission components or flywheels to optimize the volume, mass, number of parts, power transfer and assembly time. For electric vehicles with built-in wheel motors the payoff is a simpler power train, higher efficiency and lower cost. Dual-function rotors may also appear in pumps, elevators, energy storages and other machinery, bringing added values and new levels of performance to these products.

The authors believe that this first book in English devoted entirely to AFPM brushless machines will serve as a textbook, useful reference and design handbook of AFPM machines and will stimulate innovations in this field.

J.F. GIERAS, R. WANG AND M.J. KAMPER

Chapter 1

INTRODUCTION

1.1 Scope

The term *axial flux permanent magnet* (AFPM) machine in this book relates only to permanent magnet (PM) machines with *disc type rotors.* Other AFPM machine topologies, e.g. *transverse flux machines,* have not been considered. In principle, the electromagnetic design of AFPM machines is similar to its radial flux PM (RFPM) counterparts with cylindrical rotors. However, the mechanical design, thermal analysis and assembly process are more complex.

1.2 Features

The AFPM machine, also called the *disc-type* machine, is an attractive alternative to the cylindrical RFPM machine due to its pancake shape, compact construction and high power density. AFPM motors are particularly suitable for electrical vehicles, pumps, fans, valve control, centrifuges, machine tools, robots and industrial equipment. The large diameter rotor with its high moment of inertia can be utilised as a flywheel. AFPM machines can also operate as small to medium power generators. Since a large number of poles can be accommodated, these machines are ideal for low speed applications, as for example, electromechanical traction drives, hoists or wind generators.

The unique disc-type profile of the rotor and stator of AFPM machines makes it possible to generate diverse and interchangeable designs. AFPM machines can be designed as single air gap or multiple air gaps machines, with slotted, slotless or even totally ironless armature. Low power AFPM machines are frequently designed as machines with slotless windings and surface PMs.

As the output power of the AFPM machines increases, the contact surface between the rotor and the shaft in proportion to the power becomes smaller.

Table 1.1. Specifications of double-sided disc type AFPM brushless servo motors manufactured by *E. Bautz GmbH*, Weiterstadt, Germany

Quantity	S632D	S634D	S712F	S714F	S802F	S804F
Rated power, W	680	940	910	1260	1850	2670
Rated torque, Nm	1.3	1.8	2.9	4.0	5.9	8.5
Maximum torque, Nm	7	9	14	18	28	40
Standstill torque, Nm	1.7	2.3	3.5	4.7	7.0	10.0
Rated current, A	4.0	4.9	4.9	6.6	9.9	11.9
Maximum current, A	21	25	24	30	47	56
Standstill current, A	5.3	6.3	5.9	7.8	11.7	14.0
Rated speed, rpm	5000	5000	3000	3000	3000	3000
Maximum speed, rpm	6000	6000	6000	6000	6000	6000
Armature constant, V/1000 rpm	23	25	42	42	42	50
Torque constant, Nm/A	0.35	0.39	0.64	0.64	0.64	0.77
Resistance, Ω	2.5	1.8	2.4	1.5	0.76	0.62
Inductance, mH	3.2	2.8	5.4	4.2	3.0	3.0
Moment of inertia, $kgm^2 \times 10^{-3}$	0.08	0.12	0.21	0.3	0.6	1.0
Mass, kg	4.5	5.0	6.2	6.6	9.7	10.5
Diameter of frame, mm	150	150	174	174	210	210
Length of frame, mm	82	82	89	89	103	103
Power density, W/kg	151.1	188.0	146.8	190.9	190.7	254.3
Torque density, Nm/kg	0.289	0.36	0.468	0.606	0.608	0.809

Careful attention must be given to the design of the rotor-shaft mechanical joint as this is usually the cause of failures of disc type machines.

In some cases, rotors are embedded in power-transmission components to optimise the number of parts, volume, mass, power transfer and assembly time. For electric vehicles (EVs) with built-in wheel motors the payoff is a simpler electromechanical drive system, higher efficiency and lower cost. Dual-function rotors may also appear in pumps, elevators, fans and other types of machinery, bringing new levels of performance to these products.

Most applications use the AFPM machine as a d.c. brushless motor. Encoders, resolvers or other rotor position sensors are thus a vital part of brushless disc motors.

Table 1.1 shows specifications of AFPM brushless servo motors rated up to 2.7 kW, manufactured by *E. Bautz GmbH,* Weiterstadt, Germany.

1.3 Development of AFPM machines

The history of electrical machines reveals that the earliest machines were axial flux machines (M. Faraday, 1831, anonymous inventor with initials P.M., 1832, W. Ritchie, 1833, B. Jacobi, 1834). However, shortly after T. Davenport (1837) claimed the first patent [66] for a radial flux machine, conventional radial flux machines have been widely accepted as the mainstream configuration for electrical machines [30, 49].

The first primitive working prototype of an axial flux machine ever recorded was M. Faraday's disc (1831) - see Numerical Example 1.1. The disc type construction of electrical machines also appears in N. Tesla's patents, e.g. U.S. patent No. 405 858 [225] entitled *Electro-Magnetic Motor* and published in 1889 (Fig. 1.1). The reasons for shelving the axial flux machine were multifold and may be summarised as follows:

- strong axial (normal) magnetic attraction force between the stator and rotor;
- fabrication difficulties, such as cutting slots in laminated cores and other methods of making slotted stator cores;
- high costs involved in manufacturing the laminated stator cores;
- difficulties in assembling the machine and keeping the uniform air gap.

Although, the first PM excitation system was applied to electrical machines as early as the 1830s, the poor quality of hard magnetic materials soon discouraged their use. The invention of Alnico in 1931, barium ferrite in the 1950s and especially the rare-earth neodymium-iron-boron (NdFeB) material (announced in 1983) have made a *comeback* of the PM excitation system possible.

It is generally believed that the availability of high energy PM materials (especially *rare earth* PMs) is the main driving force for exploitation of novel PM machine topologies and has thus revived AFPM machines. Prices of rare-earth PMs have been following a descending curve in the last decade of the 20th century with a sharp decline in the last three years. A recent market survey shows that the NdFeB PMs can now be purchased in the Far East for less than U.S.$ 20 per kilogram. With the availability of more affordable PM materials, AFPM machines may play a more important role in the near future.

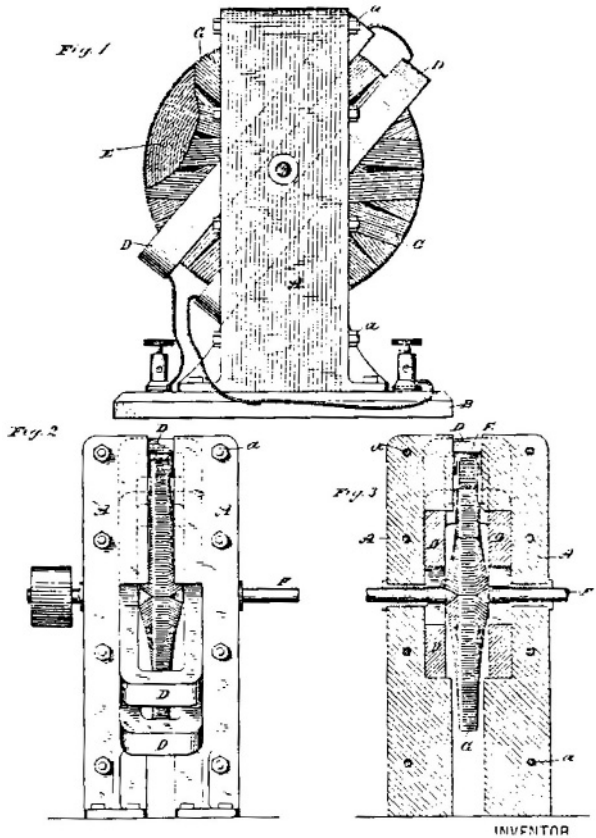

Figure 1.1. Electro-magnetic motor with disc rotor according to N. Tesla's patent No. 405 858, 1889 [225].

1.4 Types of axial flux PM machines

In principle, each type of a radial flux machine should have its corresponding axial flux (disc type) version. In practice, disc type machines are limited to the following three types:

- PM d.c. commutator machines;
- PM brushless d.c. and synchronous machines;
- induction machines

Similar to its RFPM counterpart, the AFPM d.c. commutator machine uses PMs to replace the electromagnetic field excitation system. The rotor (armature) can be designed as a *wound rotor* or *printed winding* rotor.

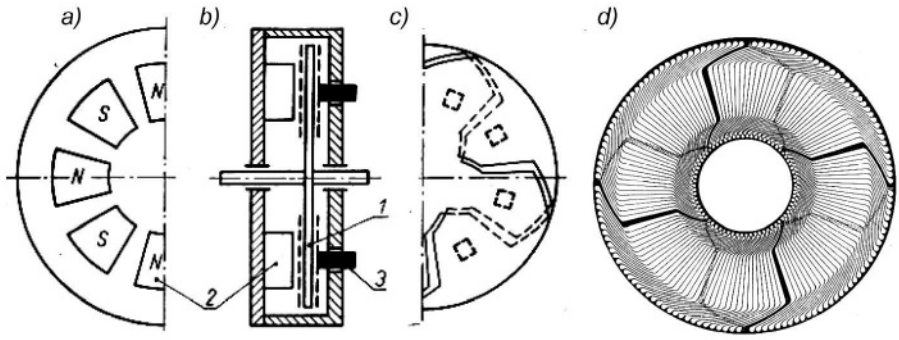

Figure 1.2. AFMPM 8-pole d.c. commutator motor with printed rotor winding: (a) stator with PMs, (b) cross section, (c) rotor (armature) windings and brushes, (d) construction of $2p = 8$ winding with 145 bars. 1 — rotor with double-sided printed winding, 2 — PMs, 3 — brushes.

In the wound rotor, the armature winding is made of copper wires and moulded with resin. The commutator is similar to that of the conventional type, i.e. it can be either a cylindrical or radial commutator.

The *disc-type printed armature winding motor* is shown in Fig. 1.2. The rotor (armature) does not have a ferromagnetic core and its winding is similar to the wave winding of conventional d.c. commutator machines. The coils are stamped from pieces of sheet copper and then welded, forming a wave winding. When this motor was invented by J. Henry Baudot [16], the armature was made using a similar method to that by which printed circuit boards are fabricated. Hence, this is called the printed winding motor. The magnetic flux of a d.c. printed winding commutator motor with a large air gap can be produced using cost effective Alnico magnets with high remanence.

AFPM d.c. commutator motors are still a versatile and economical choice for certain industrial, automotive and domestic applications such as fans, blowers, small EVs, power tools, appliances, etc.

Practically, d.c. brushless and a.c. synchronous machines have almost the same structure, though their theory and operation principles are somewhat different [96, 112, 172]. The main difference is in the shape of the operation current waveform (Fig. 1.3), i.e.:

- the d.c. brushless machine generates a trapezoidal EMF waveform and is operated with a rectangular line current waveform (also called a *square-wave* machine);

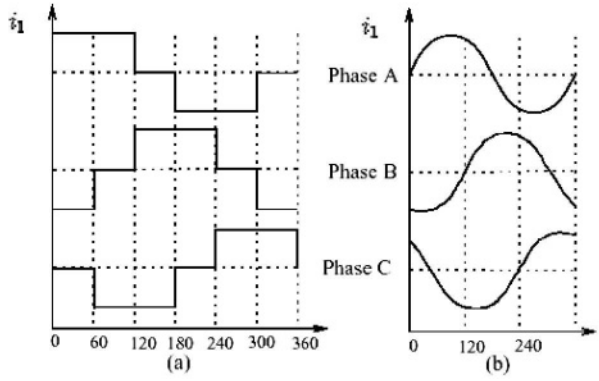

Figure 1.3. Current waveforms for AFPM brushless machines: (a) square-wave machine, (b) sinewave machine.

- the a.c. synchronous machine generates a sinusoidal EMF waveform and is operated with sinewave currents (also called a *sinewave* machine).

It is difficult to manufacture a laminated rotor with cage winding for a disc-type induction machine [148]. If the cage winding is replaced with a non-magnetic high conductivity (Cu or Al) homogenous disc or steel disc coated with copper layer, the performance of the machine drastically deteriorates. Therefore, there is little interest in disc type induction machines so far [148, 238].

1.5 Topologies and geometries

From a construction point of view, brushless AFPM machines can be designed as single-sided or double-sided, with or without armature slots, with or without armature core, with internal or external PM rotors, with surface mounted or interior PMs and as single stage or multi-stage machines.

In the case of double-sided configurations, either the external stator or external rotor arrangement can be adopted. The first choice has the advantage of using fewer PMs at the expense of poor winding utilisation while the second one is considered as a particularly advantageous machine topology [34]. The diverse topologies of AFPM brushless machines may be classified as follows:

- single-sided AFPM machines
  - with slotted stator (Fig. 1.4a)
  - with slotless stator
  - with salient-pole stator

- double-sided AFPM machines
  - with internal stator (Fig. 1.4b)
    - with slotted stator
    - with slotless stator
      - with iron core stator
      - with coreless stator (Fig. 1.4d)
      - without both rotor and stator cores

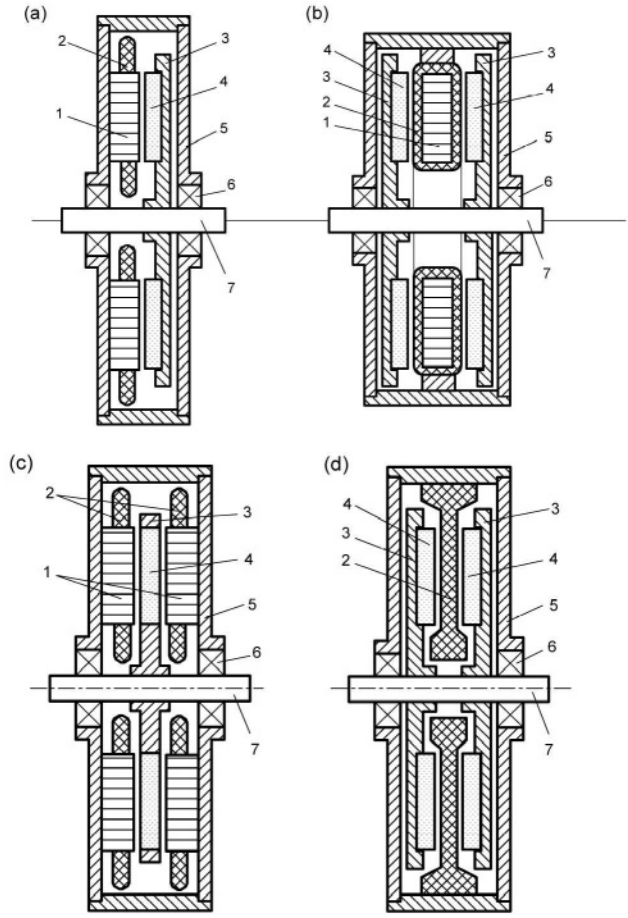

Figure 1.4. Basic topologies of AFPM machines: (a) single-sided slotted machine, (b) double-sided slotless machines with internal stator and twin PM rotor, (c) double sided machine with slotted stator and internal PM rotor, (d) double-sided coreless motor with internal stator. 1 — stator core, 2 — stator winding, 3 — rotor, 4 — PM, 5 — frame, 6 — bearing, 7 — shaft.

  - with salient pole stator (Fig. 1.5)
- with internal rotor (Fig. 1.4c)
  - with slotted stator
  - with slotless stator
  - with salient pole stator (Fig. 1.6)

- multi-stage (multidisc) AFPM machines (Fig. 1.7)

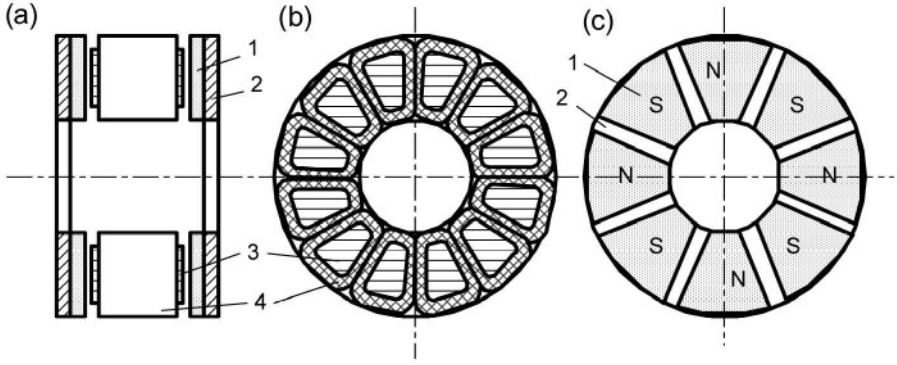

Figure 1.5. Double-sided AFPM brushless machine with internal salient-pole stator and twin external rotor [170]: (a) construction; (b) stator; (c) rotor. 1 — PM, 2 — rotor backing steel disc, 3 — stator pole, 4 — stator coil.

The air gap of the slotted armature AFPM machine is relatively small. The mean magnetic flux density in the air gap decreases under each slot opening due to increase in the reluctance. The change in the mean magnetic flux density caused by slot openings corresponds to a fictitious increase in the air gap [111]. The relation between fictitious g' and physical air gap g is expressed with the aid of Carter coefficient $k_C > 1$, i.e.

$$g' = gk_C \tag{1.1}$$

$$k_C = \frac{t_1}{t_1 - \gamma g} \tag{1.2}$$

$$\gamma = \frac{4}{\pi}\left[\frac{b_{14}}{2g}\arctan\left(\frac{b_{14}}{2g}\right) - \ln\sqrt{1+\left(\frac{b_{14}}{2g}\right)^2}\right] \tag{1.3}$$

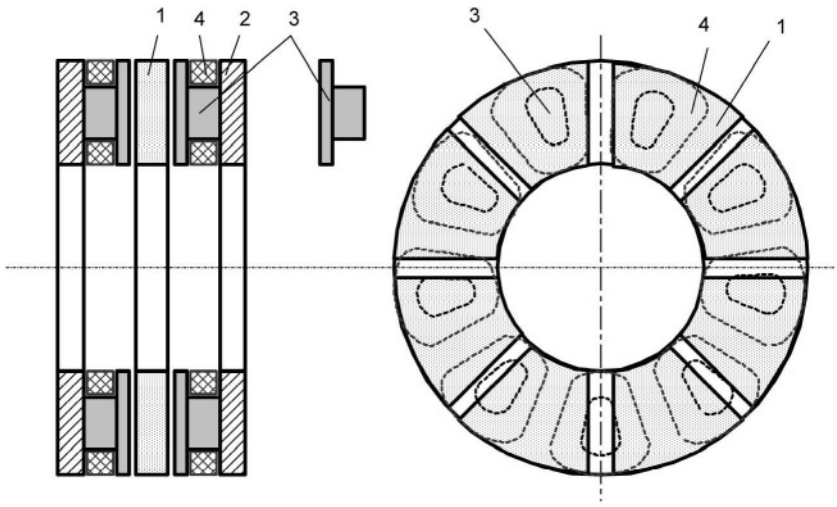

Figure 1.6. Double-sided AFPM brushless machine with three-phase, 9-coil external salient-pole stator and 8-pole internal rotor. 1 — PM, 2 — stator backing ferromagnetic disc, 3 — stator pole, 4 — stator coil.

where t_1 is the average slot pitch and b_{14} is the width of slot opening.

For AFPM machines with *slotless windings* the air gap is much larger and equal to the mechanical clearance plus the thickness of all non-magnetic materials (winding, insulation, potting, supporting structure) that is passed by the main magnetic flux. Since there are no slots, Carter coefficient $k_C = 1$. Compared to a conventional slotted winding, the slotless armature winding has advantages such as simple stator assembly, elimination of the cogging torque and reduction of rotor surface losses, magnetic saturation and acoustic noise. The disadvantages include the use of more PM material, lower winding inductances sometimes causing problems for inverter-fed motors and significant eddy current losses in slotless conductors [45].

In the double-sided, salient-pole AFPM brushless machine shown in Fig. 1.5, the stator coils with concentrated parameters are wound on axially laminated poles. To obtain a three-phase self-starting motor, the number of the stator poles should be different from the number of the rotor poles, e.g. 12 stator poles and 8 rotor poles [160, 161, 170]. Fig. 1.6 shows a double-sided AFPM machine with external salient pole stators and internal PM rotor. There are nine stator coils and eight rotor poles for a three-phase AFPM machine.

Depending on the application and operating environment, slotless stators may have ferromagnetic cores or be completely coreless. *Coreless stator* con-

figurations eliminate any ferromagnetic material from the stator (armature) system, thus making the associated eddy current and hysteresis core losses nonexisting. This type of configuration also eliminates axial magnetic attraction forces between the stator and rotor at zero-current state. It is interesting that slotless AFPM machines are often classified according to their winding arrangements and coil shapes, namely, *toroidal, trapezoidal* and *rhomboidal* forms [34, 45, 79].

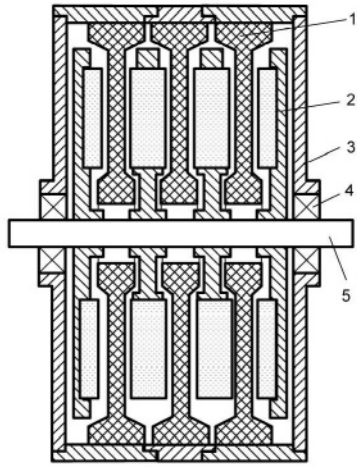

Figure 1.7. Coreless multidisc AFPM machine with three coreless stators and four PM rotor units: 1 — stator winding, 2 — rotor unit, 4 — PM, 3 — frame, 4 — bearing, 5 — shaft.

1.6 Axial magnetic field excited by PMs

A double-sided AFPM machine with twin PM rotor in *xyz* rectangular coordinate system is shown in Fig. 1.8. Assuming that the radius of curvature is higher than the pole pitch and the centre axes of the opposite rotor poles arc shifted by a linear distance x_0, the normal component of the magnetic flux density on the surface of the rotor can be described in the stationary *xyz* coordinate system by the following equations:

- at $z = 0.5d$

$$B_{mz1}(x,t) = B_0 \sum_{\nu=1}^{\infty} b_\nu \cos(\omega_\nu t \mp \beta_\nu x - \frac{\pi}{2}) \tag{1.4}$$

- at $z = -0.5d$

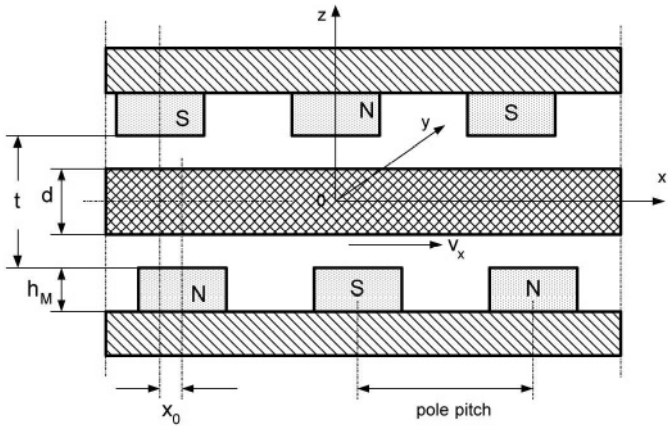

Figure 1.8. Twin-stator double-sided AFPM machine in Cartesian coordinate system.

$$B_{mz2}(x,t) = B_0 \sum_{\nu=1}^{\infty} b_\nu \cos\left[\omega_\nu t \mp \beta_\nu (x - x_0) - \frac{\pi}{2}\right] \tag{1.5}$$

where B_0 is the value of the normal component in the center axis of the North pole, and

$$\beta_\nu = \nu \frac{\pi}{\tau} \tag{1.6}$$

$$\omega_\nu = \beta_\nu v = \beta_\nu \pi D n \tag{1.7}$$

$$b_\nu = \frac{4}{\tau}\left[\frac{c_p}{c_p^2 + \beta_\nu^2}\sinh\alpha - 6\left(\frac{1}{\beta_\nu}\right)^4 \frac{1}{b_t^3}\cosh\alpha + 3\left(\frac{1}{\beta_\nu}\right)^2 \frac{2}{\tau - b_p}\cosh\alpha\right]$$

$$\times \sin(\nu\frac{\pi}{2})\sin(\nu\frac{\pi b_t}{\tau})$$

$$+\frac{4}{\tau}\left[\frac{\beta_\nu}{c_p^2 + \beta_\nu^2} + 6\left(\frac{1}{\beta_\nu}\right)^3 \frac{1}{b_t^2} - \frac{1}{\beta_\nu}\right]\cosh\alpha \sin\left(\nu\frac{\pi}{2}\right)\cos\left(\beta_\nu b_t\right) \tag{1.8}$$

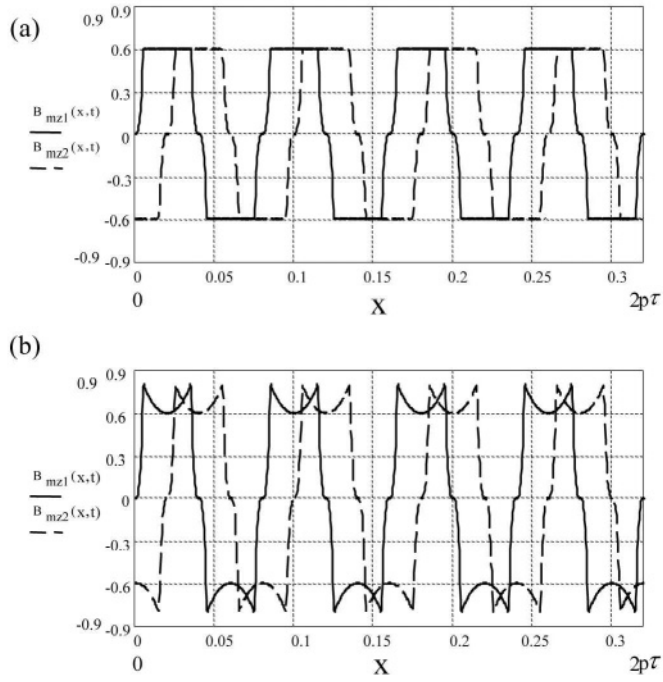

Figure 1.9. Distribution of the normal components of the magnetic flux density according to eqns (1.4), (1.5) and (1.8) for $\tau = 0.04$ m, $b_p = 0.03$ m, $B_0 = 0.6$ T, $t = 0$, $x_0 = 0.5\tau$: (a) $\alpha = 0$, (b) $\alpha = 0.8$.

$$b_t = \frac{\tau - b_p}{2} \qquad\qquad c_p = 2\frac{\alpha}{b_p}$$

In the above eqns (1.4), (1.5), (1.6), (1.7), and (1.8) $v = v_x$ is the linear speed of the rotor in the x-direction, $n = \pi D/v$ is the rotational speed in rev/s and the parameter α depends on the shape of the distribution of the normal component of the magnetic flux density (Fig. 1.9). For the flat-topped curve $\alpha = 0$ and for the concave curve (armature or eddy-current reaction) $0 < \alpha \leq 1$. The coefficient b_ν according to eqn (1.8) has been derived in [93].

The average diameter D of the PM excitation system and corresponding average pole pitch are:

$$D = 0.5(D_{out} + D_{in}) \qquad\qquad \tau = \frac{\pi D}{2p} \tag{1.9}$$

where D_{in} is the inner diameter of PMs, D_{out} is the outer diameter of PMs and $2p$ is the number of poles.

The electromagnetic field analysis in AFPM brushless machines has been discussed in e.g. [90, 91, 250, 251].

1.7 PM eddy-current brake as the simplest AFPM brushless machine

A double-sided, PM excited *eddy-current brake* with high conductivity non-magnetic disc-type rotor is one of the simplest brushless AFPM machines (Fig. 1.8). In an eddy-current brake the PM excitation system is stationary and the conductive rotor rotates at the speed n. Eqns (1.4) to (1.9) are valid since the stationary PM excitation system and rotating electric circuit (armature) are equivalent to the rotating PMs and the stationary electric circuit.

It is assumed that the eddy currents in the non-magnetic conductive disc flow only in the radial direction, i.e., in the y-direction (Fig. 1.8). Thus, the magnetic vector potential $\vec{A}$ in the disc is described by the following scalar equation (2D analysis):

$$\frac{\partial^2 A_{my\nu}}{\partial x^2} + \frac{\partial^2 A_{my\nu}}{\partial z^2} = \alpha_\nu A_{my\nu} \tag{1.10}$$

where

$$\alpha_\nu = \sqrt{j\omega_\nu \mu_0 \mu_r \sigma} = (1+j)k_\nu \tag{1.11}$$

$$k_\nu = \sqrt{\frac{\omega_\nu \mu_0 \mu_r \sigma}{2}} \tag{1.12}$$

In eqns (1.11) and (1.12) the electric conductivity σ depends on the disc temperature. The relative magnetic permeability of paramagnetic (Al) or diamagnetic (Cu) materials $\mu_r \approx 1$. The angular frequency for higher space harmonics is according to eqn (1.7) or

$$\omega_\nu = 2\pi f_\nu; \qquad f_\nu = \nu f; \qquad \nu = 1, 3, 5, \ldots \tag{1.13}$$

General solution to eqn (1.10) can be written, for example, as

$$A_{my} = \sum_{\nu=1}^{\infty} \sin(\omega_\nu t + \beta_\nu x - \frac{\pi}{2})[A_{1\nu} \exp(-\kappa_\nu z) + A_{1\nu} \exp(\kappa_\nu z)] \tag{1.14}$$

where

$$\kappa_\nu = \sqrt{\alpha_\nu^2 + \beta_\nu^2} = (a_{R\nu} + a_{X\nu})k_\nu \tag{1.15}$$

$$a_{R\nu} = \frac{1}{\sqrt{2}}\sqrt{\sqrt{4 + \left(\frac{\beta_\nu}{k_\nu}\right)^4} + \left(\frac{\beta_\nu}{k_\nu}\right)^2} \tag{1.16}$$

$$a_{X\nu} = \frac{1}{\sqrt{2}}\sqrt{\sqrt{4 + \left(\frac{\beta_\nu}{k_\nu}\right)^4} - \left(\frac{\beta_\nu}{k_\nu}\right)^2} \tag{1.17}$$

Since the currents in the disc flow only in the radial direction y, $E_{mx} = 0$ $E_{mz} = 0$ and $B_{my} = 0$ for $-0.5d \leq z \leq 0.5d$. Using the magnetic vector potential $\vec{\nabla} \times \vec{A} = \vec{B}$ and the second Maxwell's equation $\vec{\nabla} \times \vec{E} = -\partial\vec{B}/\partial t$, the remaining electric and magnetic components in the disc can be found as

$$E_{my} = -j\omega_\nu A_{my}$$

$$= -\sum_{\nu=1}^{\infty} j\omega_\nu \sin(\omega_\nu t + \beta_\nu x - \frac{\pi}{2})[A_{1\nu}\exp(-\kappa_\nu z) + A_{2\nu}\exp(\kappa_\nu z)] \tag{1.18}$$

$$B_{mx} = -\frac{\partial A_{my}}{\partial z}$$

$$= \sum_{\nu=1}^{\infty} \kappa_\nu \sin(\omega_\nu t + \beta_\nu x - \frac{\pi}{2})[A_{1\nu}\exp(-\kappa_\nu z) - A_{2\nu}\exp(\kappa_\nu z)] \tag{1.19}$$

$$B_{mz} = \frac{\partial A_{my}}{\partial x}$$

$$= \sum_{\nu=1}^{\infty} \beta_\nu \cos(\omega_\nu t + \beta_\nu x - \frac{\pi}{2})(A_{1\nu}\exp(-\kappa_\nu z) + A_{2\nu}\exp(\kappa_\nu z)) \tag{1.20}$$

The integration constants $A_{1\nu}$ and $A_{2\nu}$ can be found on the basis of equality of normal components of the magnetic flux density in the air and in the disc at $z = 0.5d$ and $z = -0.5d$, i.e.

- at $z = 0.5d$

$$\beta_\nu \cos(\omega_\nu t + \beta_\nu x - \frac{\pi}{2})[A_{1\nu}\exp(-\kappa_\nu d/2) + A_{2\nu}\exp(\kappa_\nu d/2)]$$

$$= B_0 b_\nu cos(\omega_\nu t + \beta_\nu x - \frac{\pi}{2})$$

- at $z = -0.5d$

$$\beta_\nu \cos[\omega_\nu t + \beta_\nu (x - x_0) - \frac{\pi}{2}][A_{1\nu}\exp(-\kappa_\nu d/2) + A_{2\nu}\exp(\kappa_\nu d/2)]$$

$$= B_0 b_\nu \cos[\omega_\nu t + \beta_\nu (x - x_0) - \frac{\pi}{2}]$$

There is only backward-rotating magnetic field in the air gap of an eddy-current brake, so that the terms $\beta_\nu x$ and $\beta_\nu (x - x_0)$ in eqns (1.4) and (1.5) are with the + sign. Thus,

$$A_{1\nu} = A_{2\nu} = \frac{1}{\beta_\nu} B_0 b_\nu \frac{\sinh(\kappa_\nu d/2)}{\sinh(\kappa_\nu d)} = \frac{1}{2}\frac{1}{\beta_\nu} B_0 b_\nu \frac{1}{\cosh(\kappa_\nu d/2)} \sinh(\kappa_\nu d) \tag{1.21}$$

because $\sinh(2x) = 2\sinh x \cosh x$. Putting eqn (1.21) into (1.18), (1.19) and (1.20), the particular solution to eqn (1.10) for E_{my}, B_{mx} and B_{mz} components are

$$E_{my} = -\sum_{\nu=1}^{\infty} j\omega_\nu \frac{B_0 b_\nu}{\beta_\nu} \frac{1}{\cosh(\kappa_\nu d/2)} \sin(\omega_\nu t + \beta_\nu x - \frac{\pi}{2}) \cosh(\kappa_\nu z) \tag{1.22}$$

$$B_{mx} = \sum_{\nu=1}^{\infty} \kappa_\nu \frac{B_0 b_\nu}{\beta_\nu} \frac{1}{\cosh(\kappa_\nu d/2)} \sin(\omega_\nu t + \beta_\nu x - \frac{\pi}{2}) \sinh(\kappa_\nu z) \tag{1.23}$$

$$B_{mz} = \sum_{\nu=1}^{\infty} B_0 b_\nu \frac{1}{\cosh(\kappa_\nu d/2)} \cos(\omega_\nu t + \beta_\nu x - \frac{\pi}{2}) \cosh(\kappa_\nu z) \tag{1.24}$$

The surface wave impedance for the νth space harmonic is calculated on the basis of eqns (1.22) and (1.23)

$$z_\nu = r_\nu + jx_\nu = -\mu_0\mu_r \left[\frac{E_{my}}{B_{mx}}\right]_{z=0.5d} = \frac{\alpha_\nu^2}{\sigma}\frac{1}{\kappa_\nu}\coth(\kappa_\nu\frac{d}{2})$$

$$= [(B_{R\nu}A_{R\nu} - B_{X\nu}A_{X\nu}) + j(B_{X\nu}A_{R\nu} - B_{R\nu}A_{X\nu})]\frac{k_\nu}{\sigma} \tag{1.25}$$

where

$$A_{R\nu} = \frac{\sinh(a_{R\nu}k_\nu d)}{\cosh(a_{R\nu}k_\nu d) - \cos(a_{X\nu}k_\nu d)} \tag{1.26}$$

$$A_{X\nu} = \frac{-\sin(a_{X\nu}k_\nu d)}{\cosh(a_{R\nu}k_\nu d) - \cos(a_{X\nu}k_\nu d)} \tag{1.27}$$

$$B_{R\nu} = \frac{a_{X\nu}}{0.5(a_{R\nu}^2 + a_{X\nu}^2)} \qquad B_{R\nu} = \frac{a_{R\nu}}{0.5(a_{R\nu}^2 + a_{X\nu}^2)} \tag{1.28}$$

The impedance of the disc for the νth space harmonic

$$Z_\nu = z_\nu\frac{0.5(D_{out} - D_{in})}{\tau/\nu}k_{z\nu} = \frac{\alpha_\nu^2}{\sigma}\frac{1}{\kappa_\nu}\frac{0.5(D_{out} - D_{in})}{\tau/\nu}k_{z\nu}\coth(\kappa_\nu\frac{d}{2}) \tag{1.29}$$

where D_{out} is the outer diameter of PMs, D_{in} is the inner diameter of PMs, τ is the average pole pitch (1.9) and $k_{z\nu}$ is the impedance increase factor due to circumferential currents (in the x direction). The impedance increase factor for the νth harmonic is [62]

$$k_{z\nu} = 1 + \frac{1}{\nu^2}\frac{\tau}{0.5(D_{out} - D_{in})} \tag{1.30}$$

1.8 AFPM machines versus RFPM machines

In pace with the application of new materials, innovation in manufacturing technology and improvements in cooling techniques, further increase in the power density (output power per mass or volume) of the electrical machine has been made possible. There is an inherent limit to this increase for conventional radial flux PM (RFPM) machines because of [27, 49, 96, 153, 177]:

- the bottle-neck feature for the flux path at the root of the rotor tooth in the case of induction and d.c. commutator machines or brushless machines with external rotors (Fig. 1.10);
- much of the rotor core around the shaft (rotor yoke) is hardly utilised as a magnetic circuit;
- heat from the stator winding is transferred to the stator core and then to the frame — there is poor heat removal through the stator air gap, rotor and shaft without forced cooling arrangements.

These limitations are inherently bound with radial flux structures and cannot be removed easily unless a new topology is adopted. The AFPM machine, recognised as having a higher power density than the RFPM machine, is more compact than its radial flux counterpart [26, 49, 96, 153].

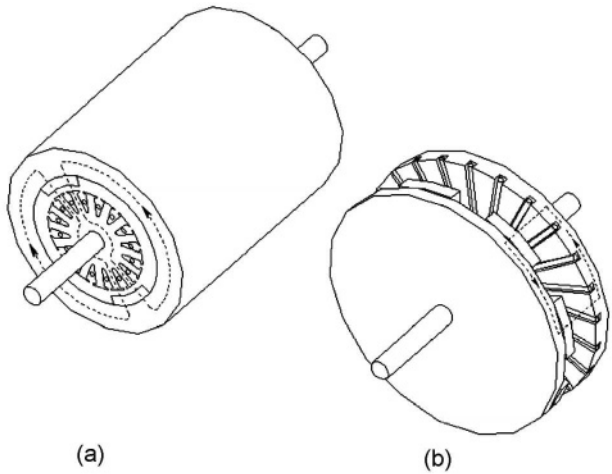

Figure 1.10. Topologies of (a) RFPM machine (b) AFPM machine.

Moreover, since the inner diameter of the core of an AFPM machine is usually much greater than the shaft diameter (see Fig. 1.4), better ventilation and cooling can be expected. In general, the special properties of AFPM machines, which are considered advantageous over RFPM machines in certain applications, can be summarised as follows [48, 96]:

- AFPM machines have much larger diameter to length ratio than RFPM machines;
- AFPM machines have a planar and somewhat adjustable air gap;

- capability of being designed to possess a higher power density with some saving in core material;
- the topology of an AFPM machine is ideal to design a modular machine in which the number of the same modules is adjusted to power or torque requirements;
- the larger the outer diameter of the core, the higher the number of poles that can be accommodated, making the AFPM machines a suitable choice for high frequency or low speed operations.

Consequently, AFPM type machines are particularly suitable for servo, traction, distributed generation and special-purpose applications where their properties offer distinct advantages over their conventional RFPM counterparts.

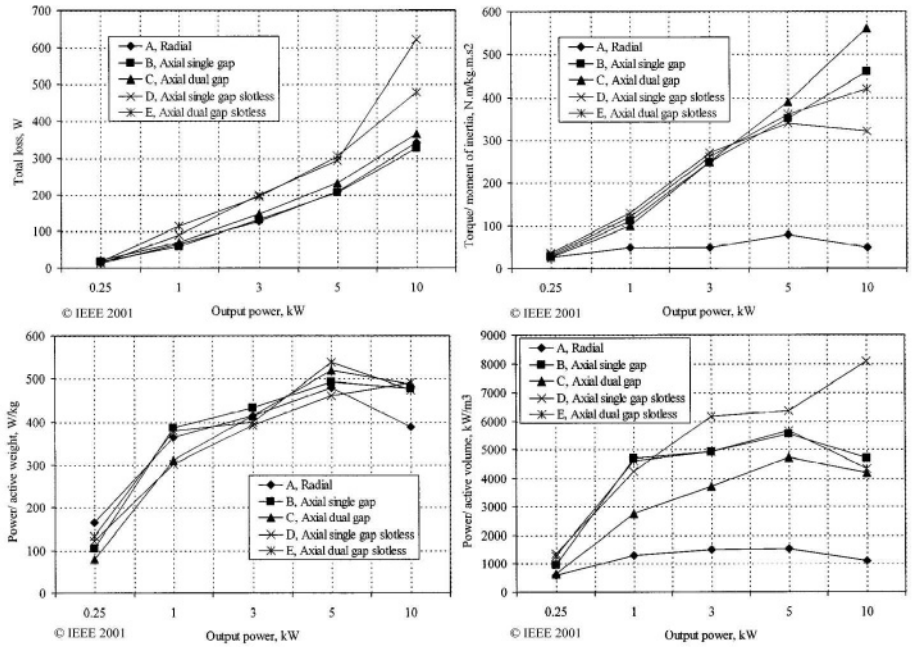

Figure 1.11. Performance comparison of RFPM and AFPM machines [214].

The quantitative comparison between traditional RFPM machine and AFPM machine is always difficult as it may raise the question of this comparison's fairness. Some published work dealt with quantitative investigations of RFPM and AFPM machine configurations in terms of sizing and power density equations [8, 49, 121, 247]. Fig. 1.11 gives the performance comparison between a conventional RFPM machine and a number of AFPM machines of different

configurations at five different power levels [214], which shows that the AFPM machine has a smaller volume and less active material mass for a given power rating than the RFPM machine.

1.9 Power limitation of AFPM machines

The power range of AFPM disc-type brushless machines is now from a fraction of a Watt to sub-MW. As the output power of the AFPM machine increases, the contact surface between the rotor and shaft becomes smaller in comparison with the rated power. It is more difficult to design a high mechanical integrity rotor-shaft mechanical joint in the higher range of the output power. A common solution to the improvement of the mechanical integrity of the rotor-shaft joint is to design a multidisc (multi-stage) machine (Fig. 1.7).

Since the scaling of the torque capability of the AFPM machine as the cube of the diameter (see eqn (2.94)) while the torque of a RFPM machines scale as the square of the diameter times the length, the benefits associated with axial flux geometries may be lost as the power level or the geometric ratio of the length to diameter of the motor is increased [174]. The transition occurs near the point where the radius equals twice the length of RFPM machine. This may be a limiting design consideration for the power rating of a single-stage disc machine as the power level can always be increased by simply stacking of disc machines on the same shaft and in the same enclosure.

Numerical example 1.1

A copper disc with its dimensions as shown in Fig. 1.12 rotates with the speed of 12 000 rpm between U-shaped laminated pole shoes of a PM. A sliding contact consisting of two brushes is used to collect the electric current generated by this primitive homopolar generator: one brush slides on the external diameter $D_{out} = 0.232$ m and the second brush is located directly below one of the poles at the distance of $0.5D_{in} = 0.03$ m from the axis of the disc. The remanent magnetic flux density of the NdFeB PM is $B_r = 1.25$ T, coercivity is $H_c = 950\,000$ A/m and height $2h_M = 0.016$ m. The thickness of the disc is $d = 0.005$ m, one-sided air gap is $g = 0.0015$ m and the width of the pole is $b_p = 20$ mm. The relative magnetic permeability of the laminated core is $\mu_r = 1000$ and the conductivity of the disc is $\sigma = 57 \times 10^6$ S/m at 20°C. The length of the flux path in the laminated core is $l_{Fe} = 0.328$ m. Find:

(a) the magnetic flux density in the air gap;

(b) the EMF between brushes;

(c) the current, if the line resistance is $R_l = 0.001\ \Omega$ and load resistance is $R_L = 0.02\ \Omega$.

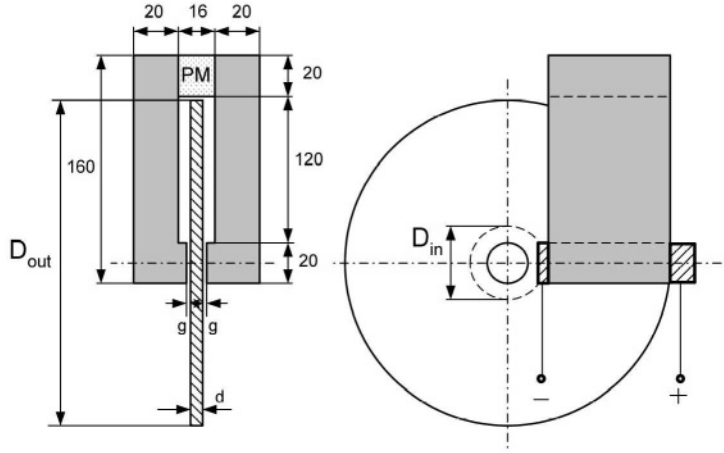

Figure 1.12. Faraday's disc: a nonmagnetic conductive disc rotating in a stationary magnetic field according to *Numerical example 1.1.*

The magnetic flux fringing effect in the air gap, the variation of magnetic permeability with the magnetic field intensity in the laminated core and brush voltage drop are neglected.

Solution

This is a homopolar type d.c. generator known as Faraday's disc and can be used as a current source, e.g. for electrolysis.

(a) Magnetic flux density in the air gap

The relative recoil magnetic permeability

$$\mu_{rrec} = \frac{1}{\mu_0}\frac{\Delta B}{\Delta H} = \frac{1}{0.4\pi \times 10^{-6}}\frac{1.25 - 0}{950000 - 0} = 1.047$$

The magnetic flux density in the air gap and saturation factor of the magnetic circuit can be found on the basis of Kirchhoff's magnetic voltage law, i.e.

$$\frac{B_r}{\mu_0\mu_{rrec}}2h_M = \frac{B_g}{\mu_0\mu_{rrec}}2h_M + \frac{B_g}{\mu_0}2g + H_{Fe}l_{Fe}$$

$$\frac{B_r}{\mu_0\mu_{rrec}}2h_M = \frac{B_g}{\mu_0\mu_{rrec}}2h_M + \frac{B_g}{\mu_0}2gk_{sat}$$

where the saturation factor of the magnetic circuit

$$k_{sat} = 1 + \frac{l_{Fe}}{2\mu_r(g + 0.5d)} = 1 + \frac{l_{Fe}}{2 \times 1000(0.0015 + 0.5 \times 0.005)} = 1.042$$